DESIGN OF A PRESSURE SWING ADSORPTION MODULE BASED ON CARBON NANOTUBES AS ADSORBENT – A MOLECULAR MODELING APPROACH

A. HEYDEN, T. DÜREN, M. KOLKOWSKI and F. J. KEIL

(Chair of Chemical Reaction Engineering, Technical University of Hamburg-Harburg, Eissendorfer Str. 38, D-21073 Hamburg, GERMANY)

The present paper describes the first sequence of the Skarstrom cycle for bed 1 to analyze the breakthrough curves and study the importance of the mass transfer resistance for the performance of the PSA process which separates a feed stream consisting of equimolar fractions of methane and ethane. The beds are filled with carbon nanotubes (CNT) of a certain inner diameter (3 nm). The adsorption bed is simulated by a one-dimensional, time-dependent dispersion model. A special feature of the present paper are the adsorption isotherms of the CH_4/C_2H_6 mixtures and the diffusivities which were calculated by molecular simulation methods.

Introduction

All adsorption separation processes involve two essential steps: a) adsorption, during which the preferentially adsorbed species are picked up from the feed gas, and b) desorption, during which these species are removed from the adsorbent, and is thus regenerated for the next cycle. The essential feature of the pressure swing adsorption (PSA) process is the removal of the adsorbed species by reducing the total pressure, rather than by raising the temperature or purging with a sweep gas. The process operates under approximately isothermal conditions. As the pressure can be changed much more rapidly than the temperature, it is possible to operate a PSA process on a much faster cycle, and thereby the throughput per unit of adsorbent bed volume is considerably increased. The major limitation is that PSA processes are restricted to components that are not too strongly adsorbed. Air separation, air drying, hydrogen purification, carbon dioxide recovery and natural gas purification are at present the most important applications of the PSA process. Detailed descriptions of this process and its applications can be found in books by Ruthven et al. [1], Yang [2], and Thomas and Crittenden [3]. An industrially employed PSA cycle is the Skarstrom cycle which in its basic form utilizes two packed adsorbent beds (see *Fig.1*). The Skarstrom cycle consists of four steps: a) pressurization, b) adsorption, c) countercurrent blowdown, and d) countercurrent purge.

In step 1, bed 1 is pressurized to the higher operating pressure with feed from the feed end (open valves: 1,3; closed valves: 2,4–9) while isolated from bed 2. During this step bed 2 is blown down from high pressure to atmospheric pressure in the opposite direction. These steps are relatively fast in most industrial processes and often have no significant influence on the performance of the entire process. In step 2 (open valves: 1,3,5,6,8; closed valves: 2,4,7,9), high pressure feed flows through bed 1. The product stream is separated from the stronger adsorbing species. The concentration front of the stronger adsorbing species reaches the exit of the bed at a far lower concentration compared to the weaker adsorbing component during this step. A fraction of the effluent stream is withdrawn as product, while the remaining gas is used to purge bed 2 at the low operating pressure. The direction of the purge flow is opposite to that of the feed flow. The purge to feed volume ratio must be at least one in order to sweep bed 2. Steps 3 and 4 follow the same sequence with the bed interchanged.

The present paper describes the first sequence of the Skarstrom cycle for bed 1 to analyze the breakthrough curves and study the importance of the mass transfer resistance for the performance of the PSA process which separates a feed stream consisting of equimolar fractions of methane and ethane. The beds are filled with carbon nanotubes (CNT) of a certain inner diameter (3 nm). The adsorption bed is simulated by a one-dimensional, time-dependent dispersion model. A
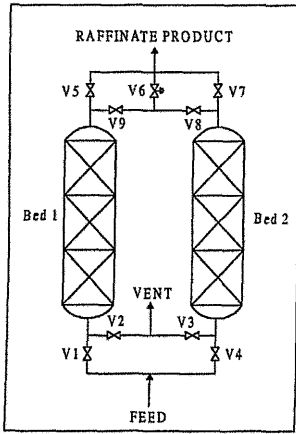

Contact information: E-mail: keil@tu-harburg.de

RAFFINATE PRODUCT

Fig.1 Schematic diagram of the basic two-bed pressure swing adsorption system.

special feature of the present paper is the adsorption isotherms of the CH_4/C_2H_6 mixtures and the diffusivities which were calculated by molecular simulation methods.

Theory

1 Grand Canonical Monte Carlo Simulations of Adsorption Isotherms

A Monte Carlo simulation (MC) generates configurations of a molecular system by making random changes to the positions of the species present (together with their orientations and conformations where appropriate). The potential energy of each configuration of the system, together with the values of other properties, can be calculated from the positions of molecules in space. The MC method thus samples from a 3N-dimensional space of the positions of N particles. In adsorption studies one would like to know the amount of material adsorbed as a function of pressure and temperature of the reservoir with which the porous material is in contact. A proper choice for adsorption studies is the grand canonical ensemble (or μVT ensemble). In this ensemble, the chemical potential μ, the volume V and the temperature T are fixed. This corresponds to an experimental setup where the adsorbed gas is in equilibrium with the gas in the reservoir. The equilibrium conditions are that the temperature and chemical potential of the gas inside and outside the adsorbent must be equal. The gas that is in contact with the adsorbent can be considered as a reservoir that imposes a temperature and chemical potential on the adsorbed gas. One has to know only the temperature and chemical potential of this reservoir to determine the equilibrium concentration inside the adsorbent. This is done with the grand-canonical ensemble. The temperature and chemical potential are set, fixed and the number of particles is allowed to fluctuate during the simulation. One should keep in mind that the pressure is related to the chemical potential

via an equation of state. Inside microporous materials the pressure is not defined. The partition function for the grand-canonical ensemble is given by [4-6]:

$$Q(\mu,V,T) = \sum_{N=0}^{\infty} \frac{\exp(\beta\mu N)q_t^N V^N}{N!} \int ds^N \exp\left[-\beta U(s^N)\right] (1)$$

and the corresponding probability density

$$N_{\mu VT}(s^N, N) \propto \frac{\exp(\beta\mu N)V^N q_t^N}{N!}\exp\left[-\beta U(s^N)\right] \quad (2)$$

with

$$\beta = \frac{1}{(T \cdot k_B)} \qquad (3)$$

$q_t^N \cdot V^N \equiv$ kinetic energy contribution of N molecules in the system. (4)

In a grand-canonical simulation, one has to sample the distribution eq. (2) by doing the following trial moves:

a) Displacement of particles. A particle is selected randomly and given a new configuration. This trial move is accepted with a probability:

$$acc(s \to s') = \min\left(1, \exp\left\{-\beta\left[U(s'^N) - U(s^N)\right]\right\}\right) \quad (5)$$

b) Insertion and removal of particles. A particle is inserted at a random position or a randomly selected particle is removed. The creation of a particle is accepted with a probability

$$acc(N \to N+1) =$$
$$= \min\left[1, \frac{q_t V}{(N+1)} \cdot \exp\{\beta[\mu - U(N+1) + U(N)]\}\right] \quad (6)$$

and the removal of a particle is accepted with a probability

$$acc(N \to N-1) =$$
$$= \min\left[1, \frac{N}{Vq_t}\{-\beta[\mu + U(N-1) - U(N)]\}\right] \quad (7)$$

Details of the implementation of eqs. (5-7) may be found in [5].

The grand-canonical MC technique can be applied to spherical molecules and simple models of nonspherical molecules. A common model to represent molecules in simulation is the united atom model. Methane is represented by a single sphere whereas chain molecules are represented by several joined spheres each denoting a methyl group of the chain molecule (e.g. ethane is represented by two joined CH_3-spheres). In more complicated cases biased sampling techniques have to be used [7]. The main feature of this more sophisticated MC method is that the trial moves are no longer completely random, instead the moves are biased in such a way that the molecule to be e.g. inserted has an enhanced probability to "fit" into the existing configuration. This approach was used for ethane in the present paper. The method to increase the speed of MC

simulations for chain molecules by MC moves is called Configuration-Bias Monte Carlo (CBMC) and was developed by Siepmann and Frenkel [7]. Further details may be found in the book by Frenkel and Smit [5] and in articles by Vlugt et al. [8-10]. The main feature of this more sophisticated MC approach is that the trial moves are no longer completely random, instead they are biased in such a way that the molecule to be, for example, inserted has an enhanced probability to "fit" into the existing configuration. No information about the present configuration of the system is used in the generation of unbiased MC trial moves. This information is used only in the acceptance criteria. The CBMC approach considerably improves the conformational sampling for molecules with complicated structures. To satisfy detailed balance, one has to change the acceptance rules. In the CBMC scheme it is common to split the total potential energy of a trial site into two parts. The first part consists of an internal, bonded, intra-molecular potential u^{int} which is used for the generation of trial orientations. The second part of the potential, the external potential u^{ext}, is used to bias the selection of a site from the set of trial sites. It should be noted that the split of the potential into u^{int} and u^{ext} is arbitrary and can be optimized for particular applications. For a new configuration n, a randomly chosen molecule of length N is regrown segment by segment. First, f trial sites for the first bead (the first atom or united atom) of the molecule are placed at random positions in the simulation box. In this work f is equal to one. This value was chosen as in the present paper only small molecules (methane and ethane) are investigated. For larger molecules f can be larger than 1. The so-called Rosenbluth weight of this segment is then [5, 8-10]:

$$w_1(n) = \sum_{j=1}^{f} \exp\left[- u_{1j}^{ext} \beta\right] \qquad (8)$$

The interaction energy u_{1j} includes all interactions of atom i with other atoms in the system. One of these trial sites is now selected with probability

$$P_{1i}^{sel}(\mathbf{b}_i) = \frac{\exp\left[- u_{1i} \beta\right]}{w_1(n)} \qquad (9)$$

For all other segments l of the molecule, k trial orientation $\mathbf{b}_i$ are generated according to the Boltzmann weight of the internal potential of that segment

$$P_{li}^{gen}(\mathbf{b}_i)d\mathbf{b} = \frac{\exp\left[- u_{li}^{int} \beta\right]d\mathbf{b}}{\int \exp\left[- u_l^{int} \beta\right]d\mathbf{b}} \qquad (10)$$

In the present paper k is set equal to six. This value can be optimized [11]. The set of k different trial segments is denoted by

$$\{\mathbf{b}\}_k = \{\mathbf{b}_1,...,\mathbf{b}_k\} \qquad (11)$$

Out of these k trial orientations one is chosen according to the Boltzmann weight of its external potential

$$P^{sel}(\mathbf{b}_i) = \frac{\exp\left[- u_{li}^{ext} \beta\right]}{\sum_{j=1}^{k} \exp\left[- u_{lj} \beta\right]} \qquad (12)$$

This procedure is repeated until the entire chain of length N has been grown. The Rosenbluth weight $W(n)$ of the new configuration is then defined as

$$W(n) = \frac{w_1(n)\prod_{l=2}^{N}\left[\sum_{j=1}^{k}\exp\left[- u_{lj}^{ext} \beta\right]\right]}{f \cdot k^{N-1}} \qquad (13)$$

The old configuration (o) is retraced in a similar way, except that for each segment only k-1 (f-1 for the first bead) trial orientations are generated with a probability given in eq. (10). The k-th (f-th) trial orientation is the old orientation. The Rosenbluth weight of the old configuration $W(o)$ is then defined as

$$W(o) = \frac{w_1(o)\prod_{l=2}^{N}\left[\sum_{j=1}^{k}\exp\left[- u_{lj}^{ext} \beta\right]\right]}{f \cdot k^{N-1}} \qquad (14)$$

where $w_1(o)$ is the Rosenbluth weight of the first segment of the old configuration. To satisfy detailed balance, the new configuration is accepted with the probability

$$acc(o \rightarrow n) = \min\left(1, \frac{W(n)}{W(o)}\right) \qquad (15)$$

In the present paper the following acceptance rules for creation and deletion were employed:

creation:

$$acc(o \rightarrow n) = \min\left\{1, \frac{f_k \beta V}{N_k(o)+1} \cdot W(n)\right\} \qquad (16)$$

deletion:

$$acc(o \rightarrow n) = \min\left\{1, \frac{N_k(o)}{f_k \beta V} \cdot \frac{1}{W(o)}\right\} \qquad (17)$$

In a trial move a molecule is displaced, and rotated in case it is not symmetrical in all directions. The distances and the angels of rotation are chosen randomly but are limited by a maximum displacement in x, y and z direction and maximum rotation angle. A good sampling of configuration space is achieved with an acceptance rate for the trial move of approximately 50%. The maximum limits of displacement are adjusted during the simulation according to this value. It should be kept in mind that a trial move in MC simulation is different from physical motion in that respect that no check for collision on the path between old and new position is done. Therefore, the maximum displacement of a molecule should always be small enough to prevent molecules from moving through the pore wall. There is no biasing-like algorithm for the trial move. Consequently, the acceptance criteria for a trial move is:

$$acc(0 \rightarrow n) = \min\{1, \exp[-\beta(u_m(n) - u_m(o))]\} \quad (18)$$

The new coordinates of each bead of the molecule after a translational move can be calculated as

$$x_m(n) = x_m(o) + \zeta \Delta x_{max} \quad (19)$$

In the rotational case an equivalent equation looks like

$$x_m(n) = x_s(o) + \mathbf{A}\nu(o) \quad (20)$$

The rotational matrix $\mathbf{A}$ is given by:

$$\mathbf{A} = \begin{pmatrix} q_0^2 + q_1^2 - q_2^2 - q_3^2 & 2(q_1q_2 - q_0q_3) & 2(q_1q_3 + q_0q_2) \\ 2(q_1q_2 + q_0q_3) & q_0^2 - q_1^2 + q_2^2 - q_3^2 & 2(q_2q_3 - q_0q_1) \\ 2(q_1q_3 - q_0q_2) & 2(q_2q_3 + q_0q_1) & q_0^2 - q_1^2 - q_2^2 + q_3^2 \end{pmatrix} \quad (21)$$

The matrix $\mathbf{A}$ is described by a quaternion of unit norm. Such a quaternion may be thought of as a unit vector in a four-dimensional space:

$$Q = (q_0, q_1, q_2, q_3) \text{ with } q_0^2 + q_1^2 + q_2^2 + q_3^2 = 1 \quad (22)$$

· If the reference frame in the center of mass of the molecule is placed in such a way that the Eulerian angles are all zero for the orientation of the old configuration, then the quaternion is:
$Q = (1,0,0,0)$. To determine the quaternion of the new orientation and therewith the rotational matrix the following scheme is used:

1. Generate two random numbers ζ_1, ζ_2 between -1 and $+1$ which satisfy the condition:

$$S_1 = \zeta_1^2 + \zeta_2^2 \leq 1 \quad (23)$$

2. Generate a second set of two random numbers ζ_3, ζ_4 between -1 and $+1$ which satisfy the same condition:

$$S_2 = \zeta_3^2 + \zeta_4^2 \leq 1 \quad (24)$$

3. The quaternion for the new orientation is:

$$Q = \left(\zeta_1, \zeta_2, \zeta_3 \cdot \sqrt{\frac{1-S_1}{S_2}}, \zeta_4 \cdot \sqrt{\frac{1-S_1}{S_2}} \right) \quad (25)$$

4. To satisfy the condition that 50% of the rotational trials are accepted, the following constraint applies:

$$1 - |\zeta_1| \leq \text{value} \quad (26)$$

whereby "value" must be adjusted such that the 50%-rule is fulfilled [5].

For molecules which consist of more than one united-atom, trials that change the internal orientation of the beads of one molecule are necessary to speed-up the simulation. There are two trials that change this internal orientation, a total regrowth trial in which the coordinates of all beads of the molecules change, and a partial regrowth trial where all beads except the first one change their coordinates. For a total regrowth the conventional CBMC scheme described above was used. In dense systems the insertion of the first bead in a total regrowth trial is unlikely, consequently the success of the entire trial becomes improbable. To be nevertheless able to change the internal orientation of the beads of one molecule the partial trial regrowth is used. Since the first bead is the same in the old and the new configuration the Rosenbluth weight of the first segment is in the old and new configuration the same and can be set equal to one:

$$w_1(o) = w_1(n) = 1 \quad (27)$$

With this change the same acceptance rule as for a total regrowth trial is employed:

$$acc(o \rightarrow n) = \min\left(1, \frac{W(n)}{W(o)}\right) \quad (28)$$

In dense systems the creation and deletion events occur, despite the use of CBMC, only with a very low probability. Therefore, so-called swap trials were introduced where the identity of a molecule changes. This trial is equivalent of deleting a molecule of species i and replacing it by a molecule j. The following acceptance rule for the swap trials was employed:

$$acc(o \rightarrow n) = \min\left(1, \frac{N_i(o)}{f_i} \cdot \frac{1}{W(o)} \cdot W(n) \cdot \frac{f_j}{N_j(o)+1}\right) \quad (29)$$

After 150,000 MC trials equilibrium was reached at all pressures. Actually, we used 250,000 equilibration steps. By doing 20 simulations of the same system, one observes that 37,500 MC steps for each pressure are enough to sample the configurational space.

2 Molecular Dynamics

In order to calculate the diffusion coefficients molecular dynamics (MD) calculations were done. The MD approach is a solution of the N-body problem of classical mechanics by integrating Newton's equations of motion for each atom k:

$$m_k \frac{\partial^2 \mathbf{r}(t)}{\partial t^2} = -\frac{\partial U(\mathbf{r})}{\partial \mathbf{r}} = \mathbf{f}_k(t) \quad (30)$$

After the starting configuration is selected, the force on each united atom is calculated and the equations of motion are integrated. The integration is done by means of the Verlet-algorithm [5,6]. First, 250,000 equilibration steps are calculated and then the time steps follow to sample equilibrium to get the desired self-diffusion coefficients by employing the Einstein-relation:

$$D_{s,k} = \frac{1}{2} \frac{\partial \langle Z_k^2(t) \rangle}{\partial t} \quad (31)$$

with

$$\langle \Delta Z_k^2(t) \rangle = \frac{1}{N} \sum_{i=1}^{N} \Delta Z_{i,k}^2(t) \quad (32)$$

The transition from self-diffusion coefficients, determined by means of MD calculations, to transport diffusion coefficients was done by a Darken factor:

$$D_{T,k} = D_{S,k}\left(\frac{\partial \ln f_k}{\partial \ln \rho_k}\right)_{\rho_j} \qquad (33)$$

To conclude, first MC simulations in the grand-canonical ensemble were done. Hereby, a specific equilibrium concentration of each component in the pore is determined at certain conditions in the bulk phase. Then a molecular dynamics calculation at the equilibrium pore concentrations was done to calculate the self-diffusion coefficients. The Darken factor can be obtained from equilibrium adsorption isotherm data. Therefore, it is necessary to calculate the derivative of the component fugacity with respect to the amount adsorbed of one component by leaving constant the amount adsorbed of the other components. In practice this is not possible since the input data of our simulations are total bulk pressure and gas fraction composition and it is hardly possible to obtain enough data at constant amount adsorbed of one component to calculate an accurate derivative. As a result Jacobian Transformations were used [12]. With the help of Jacobian Transformations, eq. (34), the derivative at constant amount adsorbed of one component can be replaced by multiple derivatives with respect to the input data. This facilitates greatly the calculation of accurate derivatives.

$$\left(\frac{\partial \ln f_k}{\partial \ln \rho_k}\right)_{\rho_j} = \frac{\partial(\ln f_k, \ln \rho_j)}{\partial(\ln \rho_k, \ln \rho_j)} =$$

$$= \frac{\dfrac{\partial(\ln f_k, \ln \rho_j)}{\partial(P, y_k)}}{\dfrac{\partial(\ln \rho_k, \ln \rho_j)}{\partial(P, y_k)}} = \frac{\begin{vmatrix} \left.\dfrac{\partial \ln f_k}{\partial P}\right|_{y_k} & \left.\dfrac{\partial \ln f_k}{\partial y_k}\right|_{P} \\[2ex] \left.\dfrac{\partial \ln \rho_j}{\partial P}\right|_{y_k} & \left.\dfrac{\partial \ln \rho_j}{\partial y_k}\right|_{P} \end{vmatrix}}{\begin{vmatrix} \left.\dfrac{\partial \ln \rho_k}{\partial P}\right|_{y_k} & \left.\dfrac{\partial \ln \rho_k}{\partial y_k}\right|_{P} \\[2ex] \left.\dfrac{\partial \ln \rho_j}{\partial P}\right|_{y_k} & \left.\dfrac{\partial \ln \rho_j}{\partial y_k}\right|_{P} \end{vmatrix}} \qquad (34)$$

In case of non-polar molecules like methane and ethane, only external interactions have to be considered. In the present paper the Lennard-Jones (L-J) potential was employed. The interaction between two Lennard-Jones sites i and j is given by the potential [5,6]:

$$U^{ij} = 4\varepsilon_{ij}\left[\left(\frac{\sigma_{ij}}{r_{ij}}\right)^{12} - \left(\frac{\sigma_{ij}}{r_{ij}}\right)^{6}\right] \qquad (35)$$

The parameters σ_{ij} and ε_{ij} are obtained from the Lorentz-Berthelot mixing rules:

$$\sigma_{ij} = 0.5(\sigma_{ii} + \sigma_{jj}) \qquad (36)$$

$$\varepsilon_{ij} = \sqrt{\varepsilon_{ii} \cdot \varepsilon_{jj}} \qquad (37)$$

The L-J potential is an effective pairwise additive potential. The interaction energy between every L-J site with all other L-J sites must be summed up:

$$U(r) = \sum_{i<j}\sum U^{ij}(r_{ij}) \qquad (38)$$

The following L-J parameters were used: CH_4 ($\sigma = 3.81$ Å, $\varepsilon/k_B = 148.1$ K), CH_3-group ($\sigma = 3.75$ Å, $\varepsilon/k_B = 98$ K).

With the usage of a cut-off radius for the potential energy the computation time can be considerably shortened. In the present paper the so-called tail-corrected L-J potential was used for the GCMC calculations [5,6]. For the MD calculations the potential was truncated and shifted, such that the potential vanishes at the cut-off radius:

$$U^{trunc}(r) = \begin{cases} U(r) - U(r_c) & r \leq r_c \\ 0 & r > r_c \end{cases} \qquad (39)$$

Periodic boundary conditions and the minimum image convention [5,6] were employed along the pore axis.

3 Model of the Adsorber Bed

For the PSA module a one-dimensional adsorber model was used. The mass balance for each component can be written at all operating conditions of the Skarstrom cycle as:

$$\frac{dc_k}{dt} = -\left(u\frac{\partial c_k}{\partial z} + c_k\frac{\partial u}{\partial z}\right) - \frac{1-\varepsilon}{\varepsilon}\rho_B \cdot \frac{\partial \overline{q}_k}{\partial t} + D_{ax}\frac{\partial^2 c_k}{\partial z^2} \quad (40)$$

Assuming that the axial pressure drop is negligible, the sum of the gas concentrations of all components is constant and no function of the axial coordinate:

$$\sum_k c_k = C \neq f(z) \qquad (41)$$

Under this condition, the overall mass balance during the high-pressure adsorption and low-pressure purge steps, where the total pressure is approximately constant, looks like:

$$C \cdot \frac{\partial u}{\partial z} + \frac{1-\varepsilon}{\varepsilon} \cdot \rho_B \sum_k \frac{\partial \overline{q}_k}{\partial t} = 0 \qquad (42)$$

Augmented by an appropriate mass transfer model, eqs. (40-42) form a set of equations which describe the time evolution of the concentration front of each component. For the mass transfer two models were used. First, for comparison, the rather unrealistic equilibrium model, which assumes that the average amount adsorbed per unit volume pellet is equal to the equilibrium amount adsorbed at the concentration of the surrounding gas phase:

$$\frac{\partial \overline{q}_k}{\partial t} = \frac{\partial q_k^*}{\partial t} = \frac{\partial q_k^*}{\partial c_k} \cdot \frac{\partial c_k}{\partial t} \qquad (43)$$

Second, a linear driving force model was employed, which gives a quite realistic description of the adsorption kinetics:

Table 1 Operating conditions and design parameters of the PSA process simulations.

Molar ratio of CH₄/C₂H₆ in feed	50/50
Feed mole flow	4 mol/s
Adsorption pressure	10 bar
Desorption pressure	1 bar
Temperature	300 K
Purge to feed volume ratio	2
Bed length	2 m
Bed diameter	0.4 m
Bed porosity	0.4
Duration of high pressure feed	140 s
Duration of low pressure purge	140 s
Representative pore diameter of the pellets	3 nm
Pellet density	1500 kg/m³
Pellet diameter	0.004 m

$$\frac{\partial \overline{q}_k}{\partial t} = k_k \left(q_k^* - \overline{q}_k \right) \qquad (44)$$

where the Glueckauf constant k_k [13]

$$k_k = \frac{15 D_{e,k}}{R_p^2} \qquad (45)$$

was introduced. The equilibrium adsorption data, q_k^*, were obtained from configurational bias MC calculations and the diffusivities from MD and MC calculations (see below). The axial dispersion coefficient, D_{ax}, was estimated by a correlation from Wen and Fan [14]:

$$\frac{1}{Pe_{ax,p}} = \frac{0.3}{Re_p \cdot Sc} + \frac{0.5}{1 + 3.8/(Re_p \cdot Sc)} \qquad (46)$$

for $0.008 < Re_p < 400$ and $0.28 < Sc < 2.2$ where

$$Pe_{ax,p} = \overline{u} \cdot d_p / D_{ax} \quad \text{and} \quad Re = \frac{\overline{u} d_p \cdot \rho}{\eta} \qquad (47)$$

The dynamic gas viscosity was estimated by a correlation from Lucas [15], and the diffusion coefficient in the Schmidt number was approximated by a correlation from Dawson et al. [16]. It was assumed that the axial dispersion coefficient is constant during the adsorption and desorption step, respectively. Therefore, the axial dispersion coefficient is only calculated for the conditions at the entrance of the adsorption bed. To sum up, the following assumptions were made in the model:

1. The cycle is isothermal.
2. There are no radial velocity or composition gradients.
3. The axial pressure drop is negligible.
4. The whole adsorbent is utilized during the feed and purge steps.
5. The pressure is constant during the feed and purge steps.
6. The dead volume at the adsorber entrance and exit is negligible.
7. The pressurization with feed and blowdown are so fast that there is no adsorption or desorption during this step. This is the so-called "frozen solid"

assumption. Pressurization and blowdown can be modelled as a pressure step.
8. Mass transfer resistance:
   a) Equilibrium model (no mass transfer resistance)
   b) Linear driving force model (LDF)
9. The ideal gas law is assumed.
10. The effective pore diffusion coefficient and axial dispersion coefficient are assumed to be constant during the adsorption and desorption step, respectively.

Assumption number one is common for PSA simulations, although it is known that in general the heats of adsorption are not negligible and temperature differences in the adsorption bed of more than 30 K occur in some processes [2]. Assumptions two to six provoke no severe simplifications. The most severe assumption is number seven, the "frozen solid" assumption. The pressurization and countercurrent depressurization steps can be of comparable duration as the adsorption and desorption steps. Assumption number eight specifies the mass transfer models employed. Assumption number nine is fulfilled for the desorption step at 1 bar. During the adsorption step at 10 bar, deviations of up to 5% in calculating the concentration can occur, since the compressibility factor reaches down to 0.95 for ethane. The last assumption results from the fact that the present authors simulated effective pore diffusion coefficients for methane, ethane mixtures at a total pressure of 10 bar and a bulk composition of 90 mol-% methane.

The model equations were solved by the method of lines, whereby the length coordinates were discretized and the time evolution was found by a Runge-Kutta 4th order integration. For the adsorption step the initial condition was an empty bed (unloaded CNT, $q_{k,j}(t = 0) = 0$) with a constant composition in the gas phase inside the tube of $c_{C_2H_6}(t = 0) = c_{CH_4}(t = 0) = 200.5$ mol/m³. The boundary conditions were a constant gas composition at the inlet $c_{C_2H_6}(z = 0) = c_{CH_4}(z = 0) = 200.5$ mol/m³, no concentration and velocity gradients at the outlet and a constant feed velocity at the inlet of $u(z = 0) = 4\dot{n}_{ads} / (\pi d_B^2 \varepsilon C) = 0.198$ m/s were assumed. For the desorption step, the initial load of the bed is identical to the last bed load in the adsorption step. For the gas phase the initial concentration of each component is a tenth of the concentration at the end of the adsorption step ($p_{ads} = 10 p_{des}$). The boundary conditions for the inlet, now at $z = L$, are for the velocity $u(z = L) = -0.396$ m/s and for the concentration $c_{CH_4}(z = L) = 40.1$ mol/m³, $c_{C_2H_6}(z = L) = 0$. Pure methane is used for purging. Furthermore, it was required that at the outlet (now $z = 0$), no concentration or velocity gradients exist. The operating conditions are presented in *Table 1*.

4 The carbon nanotube

Carbon nanotube (CNT) is the name of ultra thin carbon fibre with nanosize diameter (1 to 4 nm). The structure

Table 2 Calculated effective diffusion coefficients of methane and ethane in a CNT of 3 nm diameter. The temperature is 300 K, the total pressure 10 or 1 bar, respectively. The bulk mole fraction of methane is 0.9.

y_{CH_4}	$D_{e,CH_4} / [10^{-4} cm^2/s]$ at 1 bar	$D_{e,C_2H_6} / [10^{-4} cm^2/s]$ at 1 bar	$D_{e,CH_4} / [10^{-4} cm^2/s]$ at 10 bar	$D_{e,C_2H_6} / [10^{-4} cm^2/s]$ at 10 bar
0.9	2.70	0.301	4.36	0.742
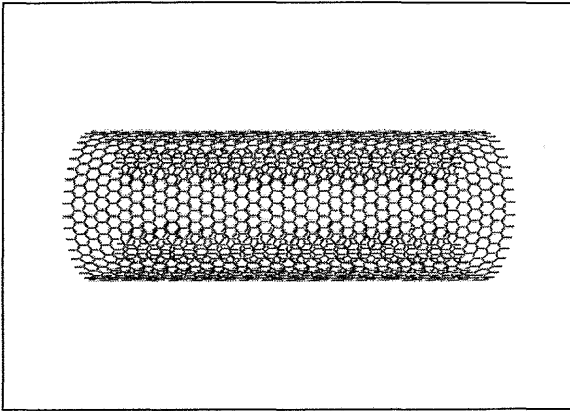
Fig.2a Carbon nanotube model with one layer zig-zag configuration. The pore illustrated has a length of 7.25 nm and a diameter of 3 nm. The hexagonal arrangement of the graphitic sheet can be observed.
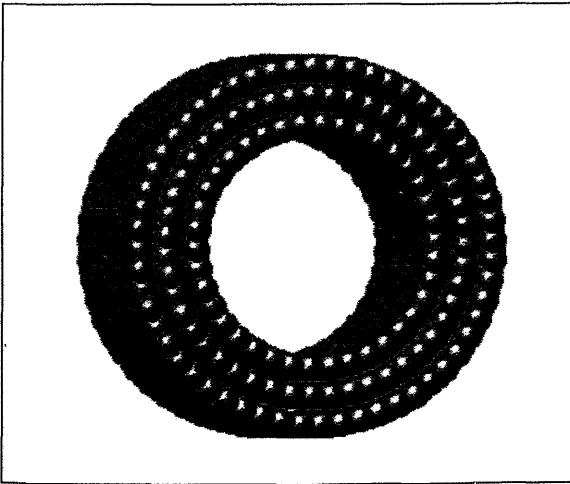
Fig.2b Carbon nanotube with three layers in zig-zag configuration.

Fig.3 Simulated amount of methane/ethane adsorbed versus bulk mole fraction of ethane in a CNT under operating conditions given in *Table 1*. (10 bar).
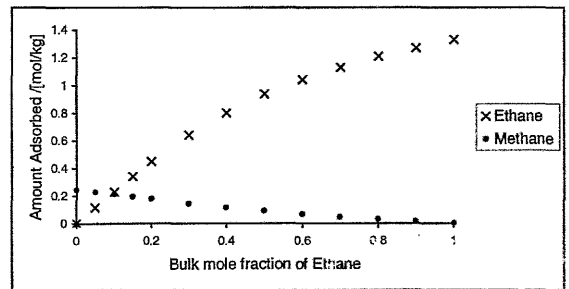

Fig.4 Like *Fig.3* for 1 bar.

$$\sigma_c = 0.34 \text{ nm and } \left(\frac{\varepsilon_c}{k_B} \right) = 28 \text{K} \qquad (48)$$

Results

To solve the equations of the PSA module (see eqs. (40-47)) one needs to know equilibrium adsorption data q_k^*, effective pore diffusion coefficients $D_{e,k}$ and an axial dispersion coefficient D_{ax}. In *Figs.3* and *4* the necessary equilibrium adsorption data at 1 and 10 bar obtained by molecular simulation are presented. The effective diffusion coefficients, approximated by the transport diffusion coefficients (eq. 33), obtained from self-diffusion coefficients multiplied by the Darken factors are given in *Table 2*. The self-diffusivities were calculated by molecular dynamics.

In *Fig.5* the concentration profiles of ethane and methane in the gas phase of the adsorber during the first high pressure adsorption step are given. In this case the equilibrium model is used for describing the mass transfer resistance that assumes an instantaneous equilibrium between the gas and solid phase. The concentration fronts are very steep, i.e. the dispersion coefficient is relatively small. One can observe that after
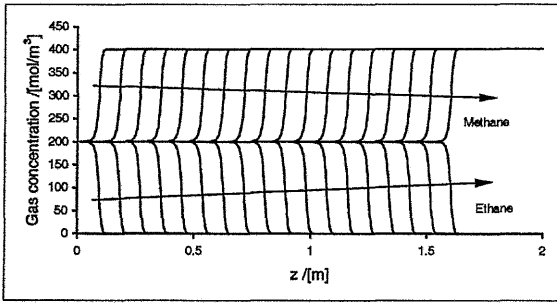
consists of enrolled graphic sheets (see *Fig.2a*). Depending on the way the sheets are enrolled one distinguishes between zig-zag, armchair and helical CNT. CNT's are further classified into multi-walled or single-walled CNT's [17]. The graphitic sheets show the hexagonal arrangement of graphite (see *Fig.2a*). Nanotubes can be used as adsorbents or molecular sieves.

In the present paper the CNT's consisted of three enrolled graphitic sheets (see *Fig.2b*) which have a distance of 0.353 nm from each other. The carbon nanotubes layers were positioned in zig-zag configuration, and the carbon atoms were kept fixed in space. The L-J potential parameters for each carbon atom were given as follows:

Fig.5 Simulated methane and ethane concentration fronts in the gas phase at various times and locations inside the bed. The concentrations are plotted every 10 s with a total time plotted of 180s. Equilibrium conditions are assumed.
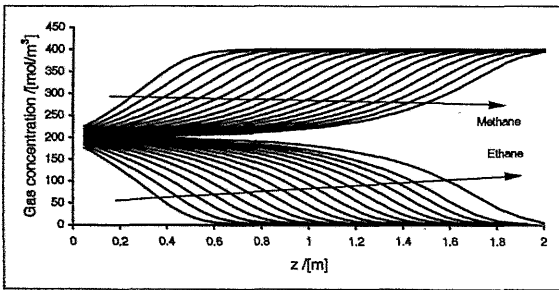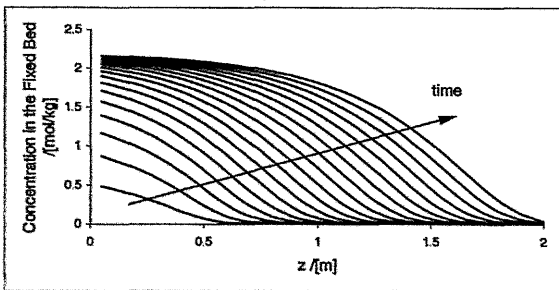

Fig.6 Simulated methane and ethane concentration fronts in the gas phase at various times and locations inside the bed. The concentrations are plotted every 10 s, the total time plotted is 180 s.

Fig.7 Simulated ethane concentration profiles adsorbed on the CNT's at various times and locations inside the bed. The concentrations are plotted every 10 s, the total time plotted is 180 s.

180 s the ethane concentration profile has moved 1.6 m away from the inlet of the adsorption bed. If one uses the linear driving force model (LDF) to describe the mass transfer kinetics between the gas and solid phase, one obtains *Fig.6*. The mass transfer resistance reduces the performance of the adsorber. *Figure 6* shows methane/ethane concentration profiles in the gas phase during the first high pressure adsorption step. One observes significant differences between *Fig.5* and *Fig.6*. First, the concentration fronts in *Fig.6* are less steep compared to the fronts in *Fig.5*. Second, the ethane concentration front has reached the outlet of the adsorption bed after 180 s in the LDF model, while for the equilibrium model the ethane concentration front
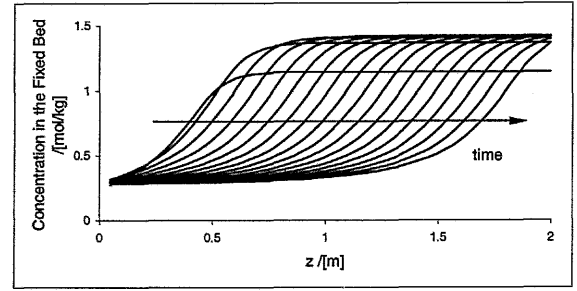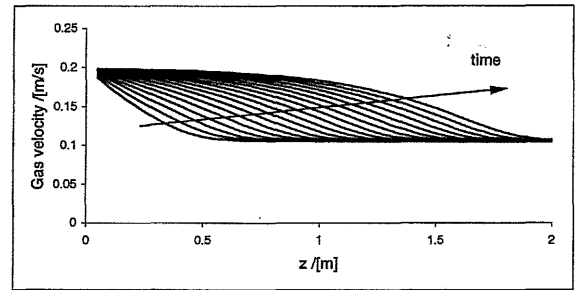

Fig.8 Like *Fig.7* for methane.

Fig.9 Simulated gas velocity in the adsorption column at various times and locations. The velocities are plotted every 10 s, the total time plotted is 180 s.

has just passed less than 80% of the bed. The mass transfer resistance reduces the performance of the adsorber. This can also be realized from the concentration profiles in the bed. *Figures 7* and *8* present the amount of adsorbed ethane and methane on the carbon nanotubes at various times and locations in the adsorber bed. As it can be observed, the amount adsorbed slowly increases with time at each location in the bed. It takes more than 100 s until 90% of the equilibrium amount of ethane has adsorbed at the inlet of the adsorber. The methane concentration in the bed increases relatively fast. The equilibrium amount of methane adsorbed is reached after 30 s. This faster equilibrium process can be explained by the approximately nine times larger pore diffusion coefficient of methane (see *Table 2*) and the smaller equilibrium amount of methane (see *Fig.3*). After 20 s methane is displaced in the bed by the slower but stronger adsorbing ethane and the methane concentration profile moves slowly out of the bed. *Figure 9* illustrates the devolution of the gas velocity in the adsorber during the high pressure adsorption step. It is shown that the velocity decreases as soon as molecules in the gas phase adsorb in the CNT pellets of our fixed bed. This results from the fact that the pressure in the adsorber is constant. The common simplification in PSA simulations, namely setting the gas velocity in the adsorber to a constant value, is not realistic in the present PSA module under the given operating conditions. *Figures 10* and *11* present the ethane and methane concentration profiles on the CNT pellets at various times and locations during the first desorption step. As expected, both the ethane and the methane concentration in the bed decrease, but the
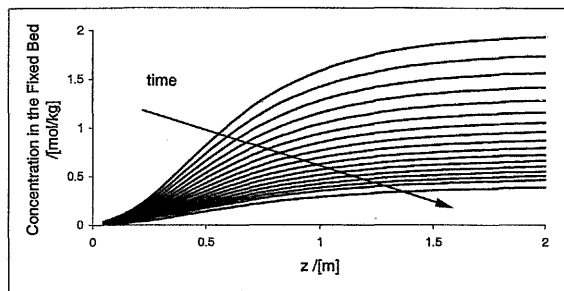
Fig.10 Simulated ethane concentration profiles adsorbed on the CNT's during the desorption step. $z = 0$ is the inlet for the purge gas. The concentrations are plotted every 10 s, the total time plotted is 180 s.

Fig.11 Like *Fig.10* for methane.

methane concentration in the bed decreases much faster than the ethane concentration since the pore diffusion coefficient of methane is far larger than the ethane pore diffusion coefficient at the pure pressure of 1 bar. After 180 s, the ethane concentration in the bed is still 20% at the outlet of the purge stream. This results from the approximately 2.5 times smaller pore diffusion coefficients at 1 bar in comparison with 10 bar. The equilibration process is much slower in the desorption step than in the adsorption step.

The adsorption characteristics is very realistic compared to published data for PSA adsorbers [1].

Conclusion

The present paper demonstrated that through a conjunction of an adsorber model with molecular simulations it is possible to simulate the behaviour of a PSA module without any experimental PSA data. The molecular simulations give far deeper and realistic insights into the molecular processes of adsorption and desorption occuring inside the porous materials compared to merely descriptive models. Realistic results compared to published experimental PSA data could be obtained.

SYMBOLS

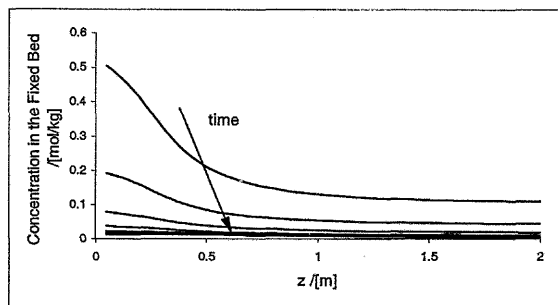|	
A	rotational Matrix
b	trial orientation
C	total gas concentration
c_k	concentration of component k
$D_{T,k}$	transport diffusion coefficient of molecule k
$D_{s,k}$	self-diffusion coefficient of molecule k
$D_{e,k}$	effective diffusion coefficient of molecule k
d_p	particle diameter
f	number of trial sites, function (eq. (41))
f_k	fugacity of component k
f	force
k	number of trial orientations
k_k	Glueckauf constant
k_B	Boltzmann's constant
m_k	molar mass of component k
N	number of molecules

o	old state
P	total gas pressure
P_{ij}	probability
Pe_{ax}	axial Peclet number
p_k	partial pressure of component k
q	coordinate of quaternion
Q	grand-canonical partition function, quaternion (eq. (22))
$\overline{q}_k$	amount adsorbed of component k per unit mass adsorbent
q_k^*	equilibrium amount adsorbed per unit mass adsorbent
q_t	part of the kinetic energy contribution of one molecule
r	vector between two points
r	distance
Re_p	particle Reynolds number
R_p	particle radius
S	auxiliary variable (eqs. (23-25))
Sc	Schmidt number
s	generalized position
T	temperature
t	time
U	potential energy
u	potential energy exerted on the system
$\overline{u}$	superficial velocity
v	relative coordinate
V	volume
w	Rosenbluth weight of a molecule segment
W	Rosenbluth weight of a configuration
x	Cartesian coordinate
y	gas mole fraction
Z	axial coordinate of molecule position in pore
z	length coordinate of adsorber bed

Greek letters

β	$\beta = 1/(k_B \cdot T)$
ε	Lennard Jones parameter, bed porosity (eqs. (39, 41))
η	dynamic viscosity
μ	chemical potential
ζ	random number between -1 and $+1$
ρ_B	bed density
ρ	gas density

ρ_k amount of k adsorbed per unit volume
σ Lennard Jones parameter

Superscripts

ext   external
gen   generating
int   internal
trunc truncated
sel   selecting

Subscripts

c   cut-off
i,j,l index
m   molecule
p   pellet
s   self, center of mass

REFERENCES

1. RUTHVEN D. M., FAROOQ S. and KNAEBEL K. S.: Pressure Swing Adsorption, VCH, New York, 1994
2. YANG R. T.: Gas Separation by Adsorption Processes, Butterworth, Stoneham, 1987
3. THOMAS W. J. and CRITTENDEN B.: Adsorption Technology and Design, Butterworth-Heinemann, Oxford, 1998
4. MCQUARRIE D. A.: Statistical Mechanics, Harper Collins Publishers, NewYork, 51, 1976
5. FRENKEL D. and SMIT B.: Understanding Molecular Simulation, Academic Press, New York, 117-118, 1996
6. ALLEN M. P. and TILDESLEY D. J.: Computer Simulation of Liquids, Clarendon Press, Oxford, 42, 1993
7. SIEPMANN J. I. and FRENKEL D.: Molecular Phys., *1992*, 75, 59-70
8. VLUGT T. J. H., MARTIN M. G., SMIT B., SIEPMANN J. I. and KRISHNA, R.: Mol. Phys., *1998*, 94, 727-733
9. VLUGT T. J. H., KRISHNA R., SMIT B.: J. Phys. Chem., *1999*, B 103, 1102-1118
10. VLUGT T. J. H.: Mol. Sim., *1999*, 23, 63-78
11. MOOIJ G. C. A. M., FRENKEL D.: Mol. Sim., *1996*, 17, 41-55
12. TESTER J. W. and MODELL M.: Thermodynamics and Its Applications, Prentice Hall PTR, New Jersey, 1997
13. GLUECKAUF E.: Trans. Faraday Soc., *1955*, 51, 1540-1548
14. WEN C. Y. and FAN L. T.: in: ALBRIGHT L. F., MADDOX R. N., MCKETTA J. J. (Eds): Chemical Processing and Engineering, Marcel Dekker, New York, 3, 1975
15. LUCAS K.: Chem.-Ing.-Techn., *1974*, 46, 157
16. DAWSON R. F., KHOURY F. and KOBAYASHI R.: AIChE J., *1970*, 16, 725-731
17. HARRIS P. J. F.: Carbon nanotubes and related structures, Cambridge University Press, Cambridge, 1999